Transient response of magnetorheological fluids: Shear flow between concentric cylinders

John C. Ulicny and Mark A. Golden

Materials and Processes Laboratory, General Motors R&D and Planning, GM R&D and Planning, MC 480-106-224, 30500 Mound Road, Warren, Michigan 48090-9055

Chandra S. Namuduri

Electrical and Controls Integration Laboratory, General Motors R&D and Planning, GM R&D and Planning, MC 480-106-390, 30500 Mound Road, Warren, Michigan 48090-9055

Daniel J. Klingenberg[a)]

Department of Chemical and Biological Engineering and Rheology Research Center, University of Wisconsin, 1415 Engineering Drive, Madison, Wisconsin 53706

(Received 11 February 2004; final revision received 27 July 2004)

Synopsis

An experimental investigation of the rheological response of magnetorheological suspensions subjected to step changes in applied magnetic field strength at fixed shear rate is reported. For small applied field strengths, the shear stress increases rapidly to a steady value. Above a critical field strength, the rapid initial increase in shear stress is followed by a slow, transient increase in stress. The critical Mason number corresponding to the critical magnetic field strength at the onset of this transient depends on the particle volume fraction as well as the shear rate. This is in contrast to a previous analysis where the critical Mason number was predicted to depend on only the particle volume fraction. The discrepancy is attributed to colloidal forces that are significant in our experimental system, but were not included in the analysis. Further comparison with the previous analysis requires either including the effects of colloidal forces, or performing experiments with systems in which colloidal forces are not important.
[DOI: 10.1122/1.1803576]

I. INTRODUCTION

Magnetorheological (MR) suspensions are typically composed of ferromagnetic particles (e.g., iron spheres) suspended in a nonmagnetizable fluid. Application of a magnetic field to these suspensions causes a dramatic increase in the apparent suspension viscosity, and the appearance of a yield stress. For concentrated suspensions, the yield stress can be on the order of 100 kPa for magnetic flux densities on the order of 1 T. The ability to

[a)]Author to who correspondence should be addressed; electronic mail: klingen@engr.wisc.edu

electronically control the apparent viscosity of MR suspensions is now being exploited in the development and commercialization of a variety of devices, such as brakes, clutches, and shock absorbers [Lewis (1999); Carlson and Sproston (2000); Corbett (2000); Kordonsky and Golini (2001); Klingenberg (2001)].

In addition to a large increase in the magnitude of the apparent rheological properties, design considerations also require knowledge of the transient rheological response following the application of a field. Numerous studies of MR suspensions and their electrical analog, electrorheological (ER) suspensions, report that the initial transient increase in stress upon application of a field is rapid, with characteristic response times in the range of roughly 1–100 ms [Johnson *et al.* (1992); Tanaka *et al.* (1992); Ginder and Ceccio (1995); Tanaka *et al.* (1995); Bullough *et al.* (1996); Nakano *et al.* (1996); Nava *et al.* (1997)]. The characteristic time depends on several factors, including the field strength, particle concentration, shear rate (for shearing flows), as well as the materials employed. In this article, we focus on an experimental investigation of the transient changes in rheological properties that occur over much longer times. Such slow transient responses can be important in the operation of devices in which the MR fluid is sheared in an applied field for long times or large strains, such as in brakes and clutches.

Vieira *et al.* (2000b) reported an experimental study of the slow transient response of ER suspensions. Suspensions were sheared at a constant shear rate and an electric field was then applied. The shear stress was monitored as a function of time. For small field strengths, the stress in the suspension increased rapidly to a steady value. For sufficiently large field strengths, the stress rapidly increased initially, and then slowly continued to increase for many tens of minutes. The authors attributed the observed slow transient response to the formation of lamellar structures within the fluid (described later). These lamellar structures were also associated with hysteretic behavior reported in a related study [Aizawa *et al.* (2000)].

The appearance of lamellar structures, or stripes, have been reported numerous times. Henley and Filisko (1999) examined the behavior of ER suspensions composed of sulfonated polystyrene ion exchange resin particles in paraffin wax subjected to dc electric fields, in shear flow between parallel disks, and between concentric cylinders. The authors sheared the suspensions at sufficiently large temperatures such that the wax was a liquid. After shearing for various times, the suspensions were cooled to freeze the wax, in order to remove the sample intact and observe the structures formed by the combination of the applied field and flow. The authors found that after shearing only for a short time (shear strains on the order of 1), the suspension formed concentrated particle stripes oriented in the flow direction. These stripes would coarsen under continued shearing. The space between the stripes was either devoid of particles, or contained particles at a much smaller concentration than that within the stripes. This and other similar studies [Filisko and Henley (2000); Vieira *et al.* (2000b)] have shown that the stripe thickness, concentration, and separation between stripes depend on the field strength, shear rate, and time of shearing.

Stripe formation has also been observed in MR fluids [Bossis *et al.* (1992; 1994), Volkova *et al.* (1999)] as well as in particle-level simulations of dipolar particles [Melrose and Heyes (1993); Martin (2000)]. In a previous study, ER and MR suspensions were modeled from a continuum perspective as coexisting particulate and fluid phases, with the objective of analyzing the field-induced migration of particles and the formation of stripes [von Pfeil *et al.* (2002; 2003)]. The particle flux was related to the divergence of the particle contribution to the stress; forms for the latter were approximated as those appropriate for amorphous, homogeneous, non-Brownian, hard-sphere suspensions. Analysis of the linearized unsteady-state particle-phase mass balance in shear flow re-

vealed that particulate stripes oriented in the flow direction should form for sufficiently large field strengths, or rather, for Mason numbers $\mathrm{Mn} \equiv \eta_c \dot{\gamma}/2\epsilon_0\epsilon_c\beta^2 E_0^2$, below a critical value Mn_c. The critical Mason number was predicted to be a function of only the particle concentration. Here, η_c is the viscosity of the continuous suspending fluid, $\dot{\gamma}$ is the shear rate, $\epsilon_0 = 8.8542\times10^{-12}$ F/m is the permittivity of free space, ϵ_c is the relative dielectric constant of the continuous phase, $\beta = (\sigma_p - \sigma_c)/(\sigma_p + 2\sigma_c)$ (for direct current fields) where σ_p and σ_c are the electrical conductivities of the particulate and continuous phases, respectively, and E_0 is the applied electric field strength. At steady state under conditions where stripes are predicted to form, analysis predicted that the suspension should be composed of particle-rich stripes oriented in the flow direction, separated by particle-free regions. Although the concentration within the stripes was predicted (and is a function of Mn), the analysis did not provide any predictions for the number or thickness of the resulting stripes. However, minimization of free energy suggests that the structure should eventually evolve to a single stripe. This analysis also did not provide any predictions for the transient rheological response that would accompany the transient structure evolution; however, since the particle concentration within the stripes increases with time after the application of a field, the apparent suspension viscosity presumably increases with time as well [von Pfeil (2002)].

In this article, we report an experimental investigation of the transient response of MR suspensions in which a magnetic field is applied to suspensions in shear flow, and interpret the results in terms of the continuum model described earlier for ER fluids. The materials employed and experimental methods are described in the following section. In Sec. III, the experimental results are presented and analyzed. For small magnetic field strengths, the apparent suspension viscosity rapidly increases to a steady value; above a critical field strength (i.e., critical current in an electromagnet), the response changes markedly, with the rapid initial increase in the apparent viscosity followed by a slow transient increase. The critical field strength corresponds to a critical Mason number. Although visual inspection of the rheometer components suggests that stripes may have formed during the course of the experiments, the critical Mason number does not depend on only the particle concentration as suggested by the continuum model. This discrepancy is possibly explained by the fact that the suspension is treated as a hard-sphere suspension in the continuum model, whereas interparticle colloidal forces are present in the suspensions employed in this study. The main conclusions from this study are summarized in Sec. IV.

II. EXPERIMENT

A. Materials

All the MR fluids used consisted of mixtures of two iron powders (all 50/50 mixtures by weight), a hydrocarbon base liquid, and fumed silica. The large particle (average 8 μm diameter) iron was BASF CM. The small particle (average 2 μm diameter) iron was BASF HS. The base liquid was Mobil SHF 21—a polyalphaolefin (PAO) of molecular

TABLE I. Compositions of MR fluids used in current step tests.

Sample code	Volume fraction iron	Fumed silica weight fraction
12MAG096	0.20	0.07
12MAG097	0.30	0.07
12MAG018	0.45	0.005

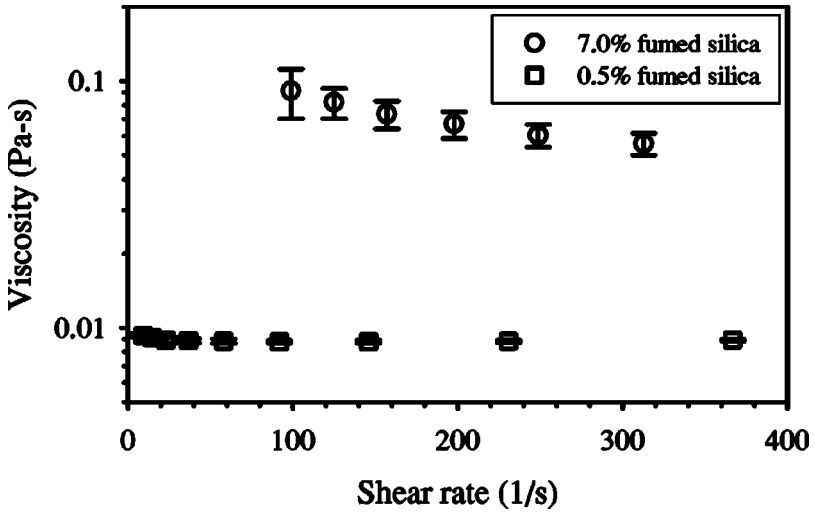

FIG. 1. Viscosity of the fumed silica in PAO suspensions (without iron particles) as a function of shear rate at 25 °C.

weight of approximately 280. The fumed silica was an untreated material (Cab-o-sil M5) from Cabot Corporation with a nominal average particle length of 0.2–0.3 μm. The compositions of each MR suspension are shown in Table I. The fumed silica concentration is given as the weight ratio of the fumed silica to the base liquid, and the iron volume fraction is based on the total volume of the suspension.

The MR fluids were prepared by blending the ingredients with a paddle mixer in a one liter container for approximately one hour. Just prior to use, each MR fluid was further mixed with a high-shear (Cowles) mixing blade for two minutes at 5000 rpm to insure uniformity and complete particle dispersal.

In Fig. 1, the viscosity of suspensions of fumed silica in PAO at the concentrations listed in Table I (i.e., the MR fluids prior to the addition of the iron particles) are plotted as a function of shear rate. The data were obtained on Bohlin VOR rheometer using a parallel disk geometry for the 7% fumed silica suspensions, and a concentric cylinder geometry for the 0.05% fumed silica suspensions. The 7% suspensions are quite thixotropic and shear thinning; samples were sheared for 30 min at each shear rate in order to reach steady state, prior to recording the viscosity. The 0.05% suspension is only weakly thixotropic and shear thinning; steady-state viscosities are obtained after shearing for roughly 1 min.

In Fig. 2, shear stress is plotted as a function of shear rate for the MR fluids employed in this study (in the absence of a magnetic field). These data were obtained with a Haake RS150 rheometer with serrated parallel disks. These samples are also thixotropic. Samples were sheared at various rates, first with increasing shear rates, and then with decreasing shear rates. Subsequent sweeps produced the same values as those of the decreasing shear rate branch of the first sweep. Data from the decreasing branch are plotted in Fig. 2. Also shown in this figure are linear regression fits of the data to the Bingham model

$$\tau = \tau_0 + \eta_{\mathrm{pl}}\dot{\gamma} \tag{1}$$

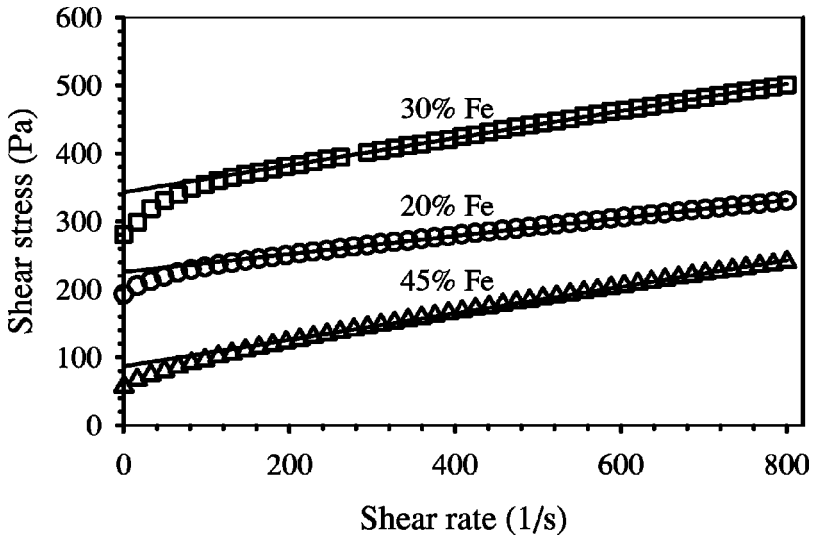

FIG. 2. Shear stress as a function of shear rate without an applied magnetic field. Solid lines represent fits of the data over the shear rate range 160–800 s^{-1}.

for data over roughly the range of shear rates explored in the step experiments ($110 \lesssim \dot{\gamma} \lesssim 800\,s^{-1}$). The yield stresses ($\tau_0$) and plastic viscosities (η_{pl}) obtained from these fits are tabulated in Table II.

B. Magnetic rheometer

The magnetic rheometer employed in this study is a custom-made, Couette-type (illustrated schematically in Fig. 3) with a soft iron rotor and soft iron cup containing the magnetic coil. The cup diameter is 10.195 cm, the height of the cup is 8.300 cm, and the height of the cup in contact with the fluid (in the lower portion of the cup) is 4.740 cm. The top half of the bob has a diameter of 9.906 cm, and the bottom half of the cup has a diameter of 10.005 cm. The bob diameter changes abruptly at half the height, in order to accommodate a gauss probe in the upper part of the gap. The bob and cup are constructed such that the magnetic field lines are perpendicular to the gap in approximately the upper and lower one-third of the gap; the fluid is contained in the lower half of the gap. The magnetic flux is measured in the air gap, and is assumed to be equal to the flux density within the fluid; the difference in flux density between the air gap and the fluid resulting from the difference in magnetic permeabilities of the air and the fluid, and resulting from the change in diameter of the bob, is assumed to be negligible. The magnetic circuit is designed to produce a maximum flux density of 1.5 T without saturating the soft magnetic parts of the structure.

TABLE II. Bingham parameters for the three different suspensions without an applied magnetic field.

Iron Conc. (vol %)	Silica Conc. (wt %)	τ_0 (Pa)	η_{pl} (Pa s)
20	7.0	225.4±0.8	0.132±0.002
30	7.0	342.7±0.9	0.200±0.002
45	0.5	86.5±1.4	0.195±0.003

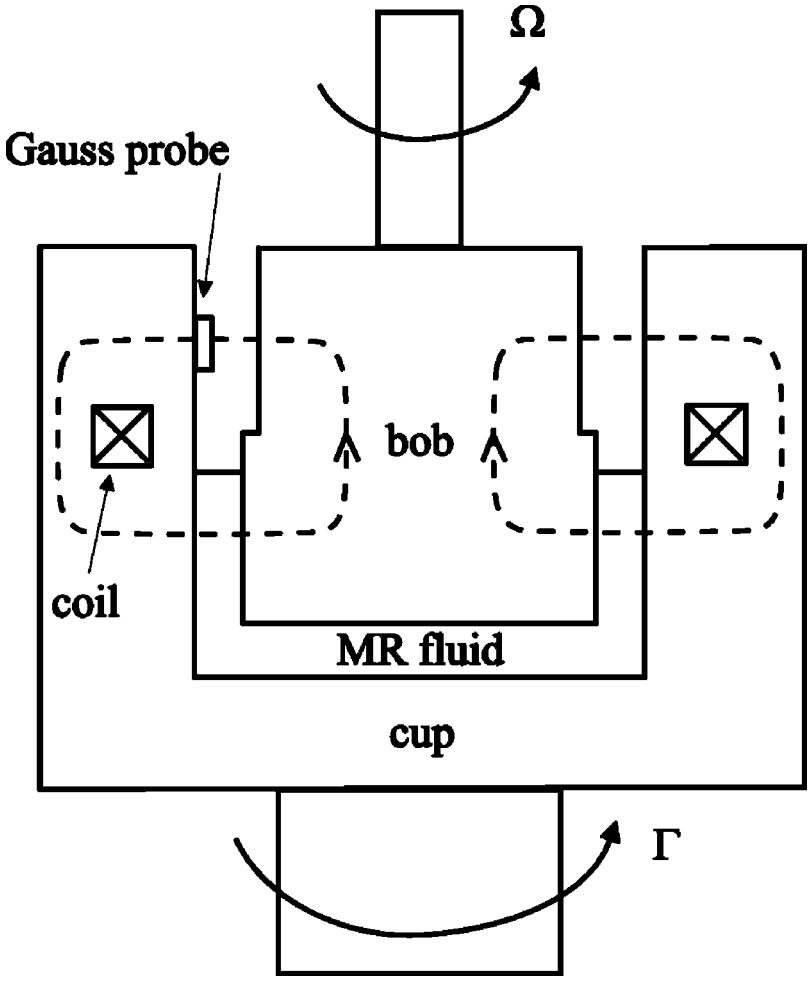

FIG. 3. Schematic diagram of the magnetic rheometer. The magnetic field lines are indicated schematically by the dashed curves.

The bob is driven by a brushless alternating current motor electric servo drive (Kollmorgen), current is supplied to the magnetic coil by a Kepco Bipolar Operational Power Supply/Amplifier (model BOP 36-12D), torque is measured by a Lebow reaction torque sensor (model 2404-500; 500 in. lb capacity), and the control and data acquisition is provided via Labview on a Windows-based personal computer. Flux density is measured in the empty upper half of the gap with the sample in place using a commercial flux probe (F. W. Bell model ST G92-020) and gaussmeter (F. W. Bell model 9200).

Time, torque, current, and rotational rate are all recorded continuously via Labview during the entire experiment. Although we originally planned to measure flux density continuously, the flux probes consistently failed to survive when the bob was rotating, so we had to settle for static flux density measurements at the beginning and end of each test.

C. Experimental procedures

A given experiment consisted of five separate procedures: mixing and distribution; flux density measurement (pre-test); yield stress versus rotational speed at zero current; current steps; and flux density measurement (post-test).

1. Mixing and distribution

The purpose of this procedure is to load the test sample of MR fluid, evenly distribute it inside the test fixture and then mix the sample so that it will be homogeneous. A previously prepared batch of MR fluid was mixed for 2 min at 5000 rpm using a high shear mixer (Cowles blade) in a 1 l container. A predetermined amount (by weight) of sample of the mixed MR fluid was then added to the magnetic rheometer cup. The bob was rotated at 4 rpm as the cup and fluid were raised to the test position so that the fluid would be evenly distributed. Mixing at 4 rpm was continued for a minimum of 5 min. The rotation speed was then raised in stages to the maximum value (160 rpm) and held for 5 min.

2. Flux density versus current (pre-test)

The purpose of this procedure is to measure the initial flux density in the MR fluid sample as a function of applied current. A flux probe is installed in the air gap of the upper half of the cup and bob assembly. The current is increased from zero in predetermined steps up to a maximum value and then decreased again to zero (at zero rotational speed). The resulting magnetic flux density values are continuously recorded during the procedure.

3. Torque versus rotational speed at zero current

The purpose of this procedure is to measure the off-state viscosity and yield stress of the MR fluid. The bob speed is increased in steps to the maximum (160 rpm) and held for 5 min to thoroughly mix the sample. The speed is then decreased to 20 rpm and held for 2 min to stabilize. The speed is then increased in steps of 20 rpm up to the maximum and held at each step for 2 min. The torque is measured continuously during the procedure.

4. Current steps

The purpose of this procedure is to measure the torque as a function of time after the current is raised to a predetermined value. The bob rotational speed Ω is increased in stages up to the maximum (160 rpm) and held for 5 min to mix the fluid. The speed is then decreased to the predetermined speed for the given test and held there for 30 s. The current is then quickly increased to a predetermined value and held for one minute. The current is then set to zero and Ω increased to the maximum and held for 5 min. The earlier sequence is repeated for a number of predetermined current values. The torque is measured continuously during the procedure.

5. Flux density versus current (post-test)

The purpose of this procedure is to determine if the flux density as a function of the current has changed during the test. The procedure is identical to that used in the pre-test procedure. The flux density is plotted as a function of current in Fig. 4 for one pre-test for each of the suspensions. A small hysteresis is present in each data set (the flux density measured with increasing currents is smaller than that measured with decreasing currents). The flux densities measured in the top and bottom of the gap without MR fluid present are also plotted in Fig. 4; these data show that there is an error of approximately

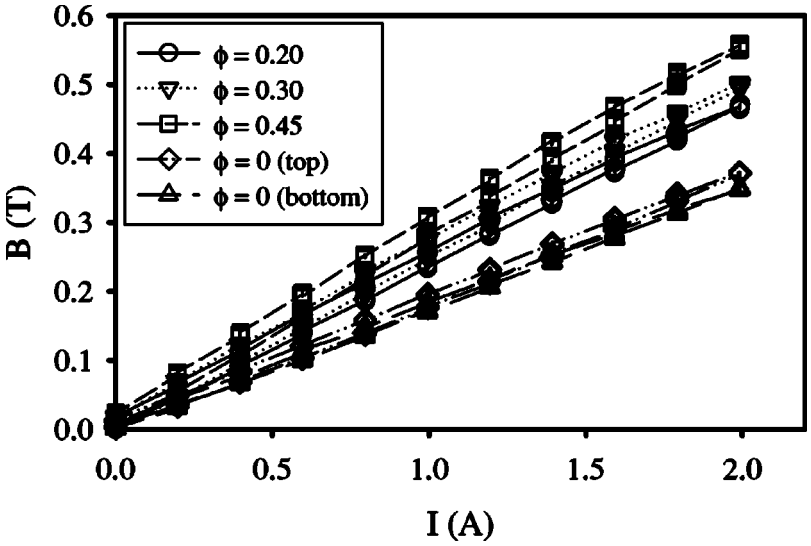

FIG. 4. Flux density as a function of current for the different suspensions employed in this study. Linear regression of the data result in the following fits (averaging data at a given current for each suspension): $\phi = 0.20$, $B = 0.2317I + 0.0132$; $\phi = 0.30$, $B = 0.2498I + 0.0122$; $\phi = 0.45$, $B = 0.2706I + 0.0153$. Also plotted are the flux densities as a function of current measured in the top and bottom of the gap without MR fluid present.

5.6% in assuming that the flux density is the same in the top and bottom of the gap. Variations among flux densities measured for each suspension in the various pre-tests and post-tests are of roughly the same magnitude as that caused by the hysteresis, and of the same magnitude as the error in assuming that the flux densities are the same in the top and bottom of the gap. Linear equations obtained from least-squares regression of all data for each suspension are presented in the caption of Fig. 4.

III. RESULTS AND DISCUSSION

Typical results for the measured torque as a function of time for different applied currents in the step experiments are illustrated in Fig. 5 for $\phi = 0.45$ and $\Omega = 160$ rpm. For small currents, the torque increases rapidly to a steady-state value (within the 2 s sampling interval), or displays a weak overshoot. For sufficiently large currents, the stress

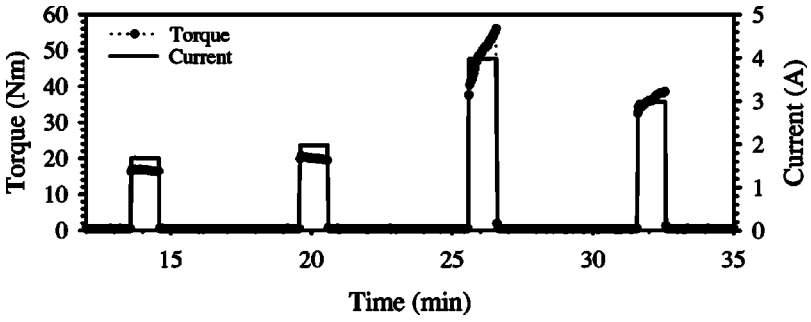

FIG. 5. Torque and current as a function of time for $\phi = 0.45$, $\Omega = 160$ rpm.

again increases rapidly, but then continues to increase more slowly. When large currents are applied for longer periods, the measured torque can continue to increase for minutes to hours.

In Fig. 6, the measured torque is plotted as a function $t-t_0$, where t is the time and t_0 is the time at which the current is applied, for different applied currents, and for different iron concentrations and rotation rates. Again, the transition from a rapid approach to steady state to a slow transient response is apparent as the applied current is increased. Varying the rotation rate at fixed concentration [Figs. 6(a) and 6(b); $\phi = 0.20$] only weakly influences the measured torque in this range. This suggests that the stress transferred in the fluid is only slightly larger than the dynamic yield stress. Varying the concentration at fixed rotation rate [Figs. 6(b) and 6(c); $\Omega = 160$ rpm] has a more significant impact, with larger torques measured for larger particle concentrations. This reflects the volume fraction dependence of the fluid yield stress (and to a small extent the volume fraction dependence of the fluid permeability; see Fig. 4).

The magnitude of the transient component of the response can be characterized by the slope S of the torque versus time data. This slope is plotted as a function of applied current for $\phi = 0.20$ and $\Omega = 160$ rpm in Fig. 7. The slopes were calculated by linear regression of the data collected while the current was applied, omitting the first and last points (in order to avoid potential errors caused by lags in the data acquisition). The data presented in Fig. 7 more clearly illustrate the transition in the temporal response of the fluid as the current is increased. For small currents, S is indistinguishable from zero, which indicates steady shear flow. For sufficiently large currents, $S > 0$, which indicates a transient increase in the measured torque.

We define a critical current I_c as the current at which slope begins to deviate from 0. The value of I_c is obtained by linear regression of the data for which $S > 0$, equating I_c with the intercept on the abscissa as illustrated in Fig. 7. Data for all runs were analyzed in this manner, and the results are summarized in Fig. 8 where I_c is plotted as a function of Ω for the three different suspensions. The critical current is insensitive to the rotation rate over the range investigated, but does depend on the particle concentration.

A transient rheological response in ER fluids has previously been attributed to stripe formation, as described in Sec. I. Photographs of the bob and cup following the sequence of applied currents for $\phi = 0.20$, $\Omega = 160$ rpm are presented in Fig. 9. Striations oriented in the direction of flow are apparent on both surfaces. While such structures are consistent with stripe formation within the fluid, this is far from conclusive evidence that stripes have indeed formed during the course of the experiment. The rheometer was disassembled in order to take these photographs, which certainly altered to the state of the fluid to some extent.

Transient increases in torque may occur, in principle, because particles migrate from the bottom of the cup into the gap (via dimagnetophoresis). Indeed, such migration was observed when the magnetic field was applied for several hours. However, for the experiments reported here in which the magnetic field was applied for only 60 s, migration from the bottom of the cup was not observed. Thus the transient increases in torque above a critical current must arise from a different mechanism.

To further analyze the possibility that the transient responses are caused by stripe formation, we compare the experimental data with predictions of the continuum model of von Pfeil *et al.* (2002, 2003). Their analysis predicts that stripes will form when the Mason number is decreased below a critical value. For our MR experiments, this would imply that stripes should form when the applied current (i.e., the applied magnetic field strength) is increased above a critical value. This prediction is consistent with the data illustrated in Fig. 7, where the transient response only occurs above a critical current.

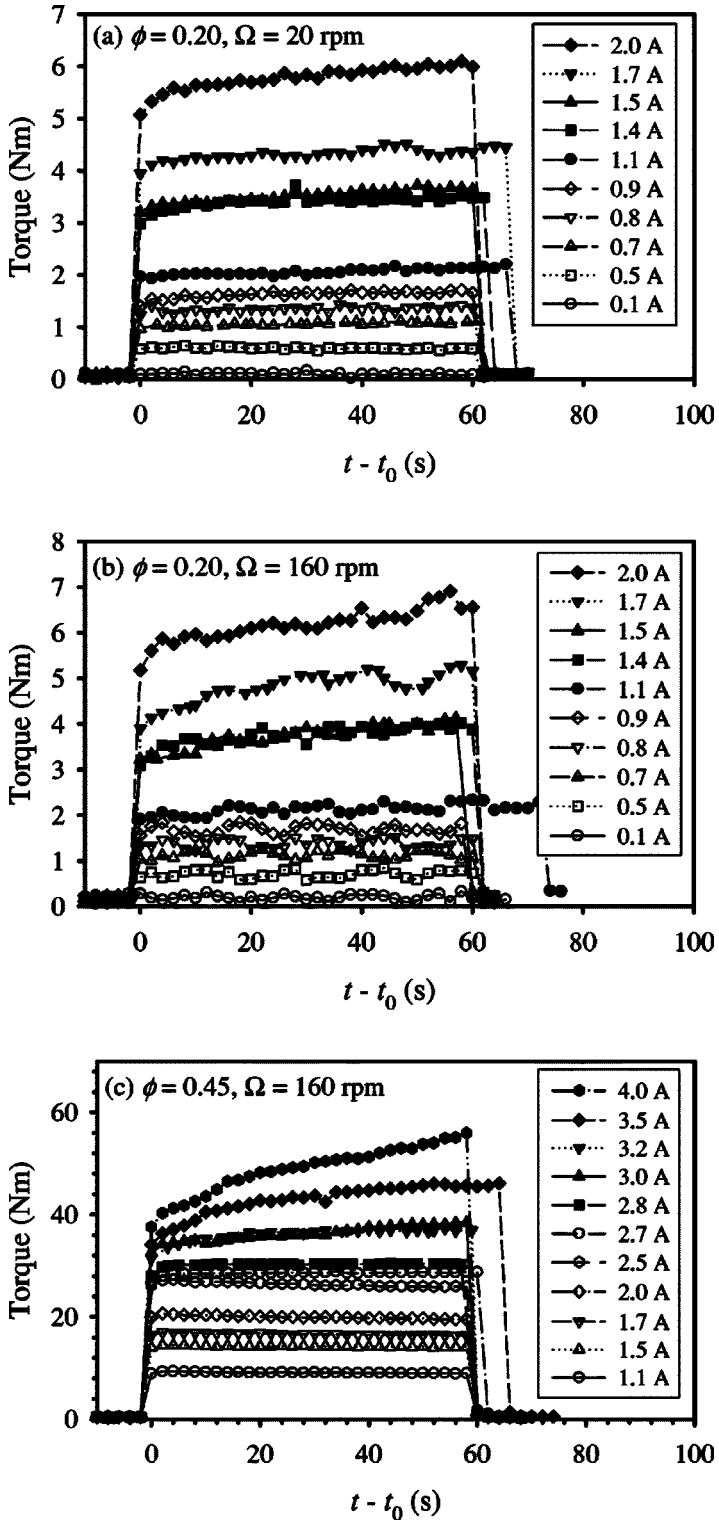

FIG. 6. Torque as a function of time (after the current has been applied) for different values of the applied current. (a) $\phi = 0.20$, $\Omega = 20$ rpm; (b) $\phi = 0.20$, $\Omega = 160$ rpm; (c) $\phi = 0.45$, $\Omega = 160$ rpm.

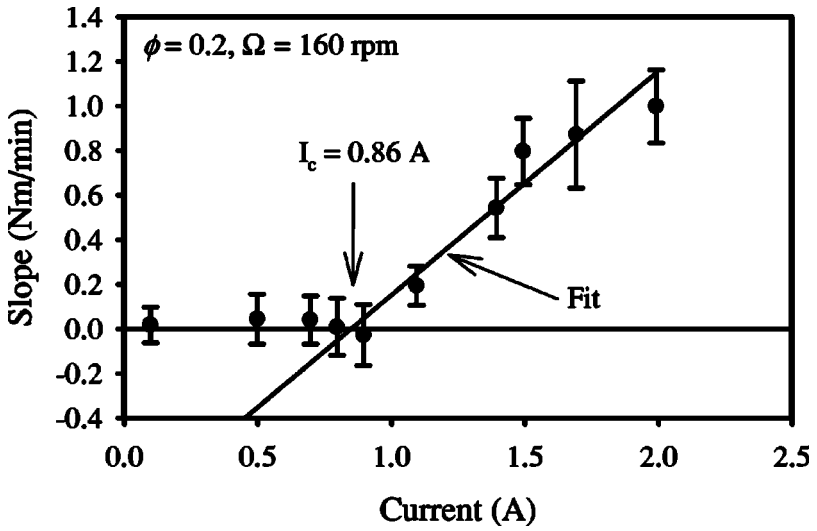

FIG. 7. Slope as a function of current for $\phi = 0.20$, $\Omega = 160$ rpm. The fit is obtained by linear regression for all points for which the slope is greater than zero.

The analysis presented by von Pfeil *et al.* also predicts that the critical Mason number should depend only on the particle concentration. To test this prediction, we must first determine the Mason numbers for our various experiments. For MR fluids, we define the Mason number

$$\mathrm{Mn} \equiv \frac{\eta_c \dot{\gamma}}{2\mu_0 \mu_c \beta^2 H_0^2}, \tag{2}$$

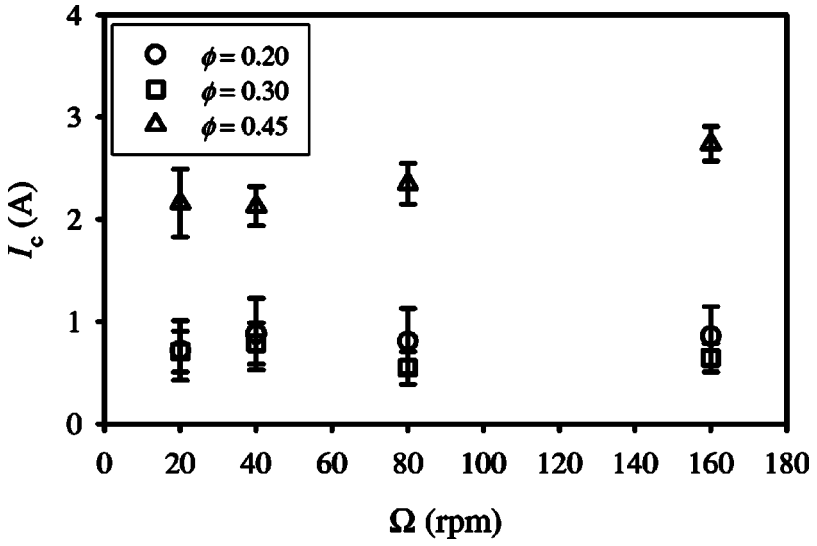

FIG. 8. Critical current as a function of Ω for the different suspensions.

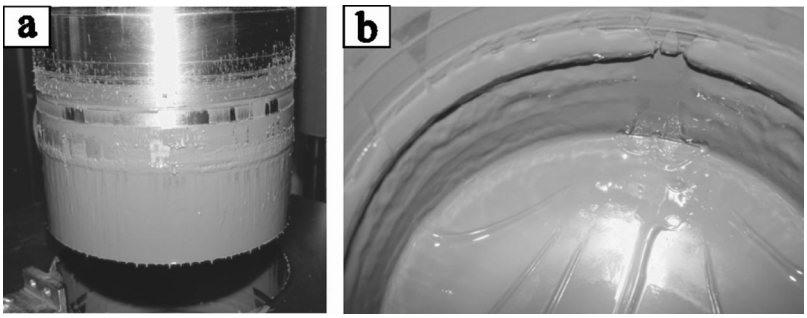

FIG. 9. Photographs of the (a) bob and (b) cup after exposing a 20% suspension to various magnetic field strengths at $\Omega = 160$ rpm. Horizontal striations are apparent on both surfaces.

where η_c is the viscosity of the continuous phase, $\dot{\gamma}$ is the shear rate, μ_0 is the magnetic permeability of free space, μ_c is the relative permeability of the continuous phase, $\beta = (\mu_p - \mu_c)/(\mu_p + 2\mu_c)$, μ_p is the relative permeability of the particles, and H_0 is the applied magnetic field strength. This definition agrees with that defined previously, within a numerical coefficient [Felt *et al.* (1996); Volkova *et al.* (2000)]. The shear rate can be determined from the rotation rate and the rheometer dimensions. For the viscosity of the continuous phase, we use the measured steady-state viscosities of the respective PAO-fumed silica suspensions at a shear rate of 300 s^{-1} (the geometric mean of the range of shear rates employed; the results of this analysis do not depend on whether or not we include the shear rate dependence of the continuous phase viscosity). However, the magnetic field strength is not measured in our experiments. We have measured the current in the electromagnet, as well as calibrations for the applied magnetic flux density B_0 as a function of current for each suspension. In the Appendix, we present a model for the field-dependent magnetic properties of isotropic suspensions, in order to determine $H_0 = B_0/\mu_0\mu_{\text{susp}}$ and β in the Mason number. We note that von Pfeil *et al.* define a critical Mason number as that at which stripes will begin to form from a homogeneous suspension. We must therefore estimate the magnetic properties and magnetic field strength in the homogeneous suspensions, prior to the formation of stripes.

Employing the magnetic properties determined in the appendix, we can calculate the critical Mason number, Mn_c, corresponding to the critical currents, I_c, in Fig. 8. In Fig. 10, Mn_c is plotted as a function of the shear rate $\dot{\gamma}$ for the three different MR fluids. The critical Mason number depends on the shear rate, which disagrees with the prediction of von Pfeil *et al.* that Mn_c should depend only on ϕ.

To understand why such a discrepancy might exist between the data and the predictions of the prior model, consider the assumptions employed by von Pfeil *et al.* They treated hard, polarizable spheres immersed in a Newtonian fluid. The suspension structure depends on the competition between the electrostatic and hydrodynamic forces acting on the particles. By dimensional analysis, the structure can only depend on the ratio of these two forces, i.e., the Mason number, and the particle volume fraction. In contrast, additional forces influence the behavior of our experimental systems. Colloidal interactions between the silica particles, and between the silica and iron particles impart non-Newtonian behavior to the MR suspensions in the absence of an applied magnetic field. Thus, we do not expect the structure to depend on only the Mason number and volume fraction; the structure should also depend on the ratio of the magnitude of the colloidal and hydrodynamic forces.

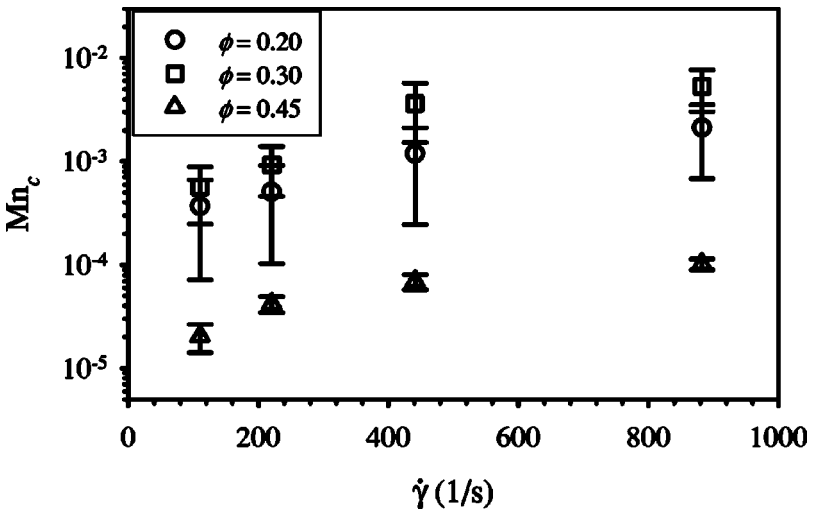

FIG. 10. Critical Mason number as a function of shear rate for the different suspensions.

We have not attempted to measure the colloidal forces acting in our systems. However, since the non-Newtonian behavior of these systems in the absence of an applied magnetic field apparently arises from these colloidal forces, we can characterize the magnitude of the colloidal forces with the yield stress τ_0 of the nonmagnetized suspensions. The ratio of the magnitudes of the colloidal and hydrodynamic forces are thus represented by the Bingham number

$$\mathrm{Bi} \equiv \frac{\tau_0}{\eta_{\mathrm{pl}}\dot{\gamma}}, \tag{3}$$

where η_{pl} is the plastic viscosity of the nonmagnetized suspensions. We expect the structure to depend on Mn, Bi, and ϕ; thus the critical Mason number should depend on Bi and ϕ.

In Fig. 11, Mn_c is plotted as a function of Bi for the different suspensions. For each suspension, Mn_c decreases with increasing Bi. We note that for these experiments, Bi varies by less than two orders of magnitude about a value of 1, suggesting that colloidal and viscous forces are of similar magnitude throughout the experiments.

While there are currently no model predictions for the dependence of Mn_c on Bi and ϕ, certain features exhibited in Fig. 11 are expected. As $\mathrm{Bi} \to 0$, we expect Mn_c to approach a ϕ-dependent asymptote (i.e., Mn_c should not diverge as $\mathrm{Bi} \to 0$) to be consistent with the continuum model. As Bi increases, the importance of colloidal forces relative to viscous forces increases. Thus we expect Mn_c to decrease, since magnetostatic forces must overcome colloidal forces of increasing strength, as well as viscous forces, in order to cause a change in the suspension microstructure. Finally, we expect Mn_c to decrease with increasing ϕ, as predicted by the continuum model (at least in the limit as $\mathrm{Bi} \to 0$). Further comparisons with the continuum model require either modification of the model to account for colloidal forces, or performing experiments with systems in which only magnetostatic and hydrodynamic forces determine the particle dynamics.

Finally, we note that the field-induced change in rheological behavior differs from that reported by Volkova *et al.* (1999). These authors examined the *steady-state* shear stress—shear rate relationship for magnetorheological (and electrorheological) suspensions. Un-

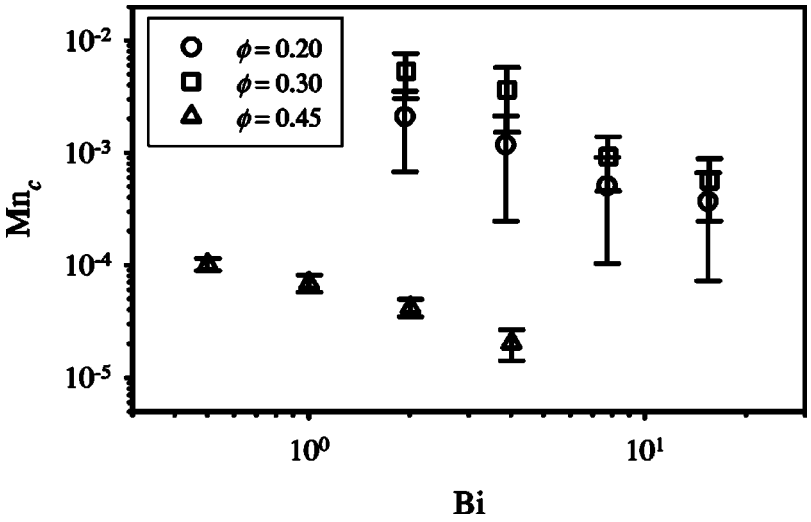

FIG. 11. Critical Mason number as a function of Bingham number for the different suspensions.

der a constant magnetic field strength, the shear stress increased with increasing shear rate as commonly observed. However, the shear stress exhibited a jump at a critical shear rate. This behavior is different than that reported here, where the onset of a transient increase in shear stress appears when the Mason number is decreased (e.g., the shear rate is decreased). It is not clear if the steady-state phenomena reported by Volkova *et al.* are related to transient behavior reported here.

IV. CONCLUSION

The rheological response of MR suspensions subjected to step changes in applied magnetic field strength at fixed shear rate was investigated experimentally. For small applied field strengths, the shear stress increased rapidly to a steady value. Above a critical field strength, the rapid initial increase in shear stress was followed by a slow, transient increase in stress. The critical Mason number corresponding to the critical magnetic field strength depends on the particle volume fraction as well as the shear rate. This is in contrast to the analysis of von Pfeil *et al.* (2003) where the critical Mason number was predicted to depend on only the particle volume fraction. The discrepancy is attributed to colloidal forces that are significant in our experimental system, but were not included in the analysis of von Pfeil *et al.* Further comparison with the previous analysis requires either including the effects of colloidal forces, or performing experiments with systems in which colloidal forces are not important.

ACKNOWLEDGMENTS

The authors wish to thank General Motors for their support of Professor Klingenberg provided as part of this cooperative project. The authors also wish to thank Keith Snavely of GM R&D for his analysis of the MR fluids used in this study, Ken Shoemaker of GM R&D for his custom programming of the data acquisition and control system for the magnetic rheometer, and David Kittipoomwong of the University of Wisconsin for his assistance with the characterization of the viscosity of the samples.

APPENDIX: MAGNETIC MODEL

In this Appendix, we derive a model for the magnetic properties of an isotropic suspension of nonlinearly magnetizable particles, in order to calculate the Mason number for flowing suspensions the instant the magnetic field is applied. According to the continuum model developed previously for ER suspensions [von Pfeil *et al.* (2002, 2003)], the value of the Mason number the instant the field is applied determines whether or not the suspension will remain homogeneous or begin to form stripes.

We treat the MR fluid as a suspension of equal sized spheres of diameter σ and field-dependent permeability μ_p immersed in a nonmagnetizable continuous phase with permeability $\mu_c = 1$. The magnetic permeability of the nonlinearly magnetizable particles is modeled with the Frohlich-Kennelly equation [Bozorth (1951); Ginder and Davis (1994)]:

$$\mu_p[H^{(p)}] = 1 + \frac{(\mu^0 - 1)M_s/H^{(p)}}{(\mu^0 - 1) + M_s/H^{(p)}}, \tag{A1}$$

where $H^{(p)}$ is the magnetic field strength inside the particles, $\mu^0 = 10^3$ is the magnetic permeability in the limit $H^{(p)} \to 0$, and M_s is the saturation magnetization ($\mu_0 M_s = 2.0\,\mathrm{T}$).

In a previous article [Shkel and Klingenberg (2001)], the magnetostatic boundary value problem of an isolated sphere in a uniform magnetic field $\mathbf{H}_0$ was solved exactly for the case of such a nonlinearly magnetizable sphere. The field strength within the sphere is related to the applied magnetic field strength by

$$\mathbf{H}^{(p)} = A_0[H^{(p)}]\mathbf{H}_0, \tag{A2}$$

where

$$A_0[H^{(p)}] = \frac{3}{\mu_p[H^{(p)}] + 2}. \tag{A3}$$

For a particle in a suspension, the point-dipole approximation was employed, where a particle's magnetization is approximated as that of an isolated sphere in a uniform magnetic field $\mathbf{H}_{\mathrm{loc}}$. Here, $\mathbf{H}_{\mathrm{loc}}$ is the local field, the sum of the applied field $\mathbf{H}_0$ plus the disturbance dipolar fields of all the other magnetized spheres. The local field ''seen'' by sphere i is

$$\mathbf{H}_{\mathrm{loc}} = \mathbf{H}_0 - \sum_{j \neq i} \mathbf{T}(\mathbf{r}_{ij}) \cdot \mathbf{m}_j, \tag{A4}$$

where $\mathbf{T}(\mathbf{r})$ is the dipole interaction tensor

$$\mathbf{T} = \frac{1}{4\pi}\left(\frac{\boldsymbol{\delta}}{r^3} - 3\frac{\mathbf{rr}}{r^5}\right), \tag{A5}$$

and $\mathbf{m}_j$ is the magnetic moment of sphere j. The magnetic moment of sphere i is related to the local field by

$$\mathbf{m}_i = \alpha_m[H^{(p)}]\mathbf{H}_{\mathrm{loc}}, \tag{A6}$$

where $\alpha_m[H^{(p)}]$ is the field-dependent magnetizability, given by

$$\alpha_m[H^{(p)}] = \frac{\pi}{6}\sigma^3\frac{\mu_p[H^{(p)}]-1}{\mu_p[H^{(p)}]+2}. \tag{A7}$$

The field strength inside the sphere is related to the local field strength by

$$H^{(p)} = A[H^{(p)}]H_{\text{loc}}, \tag{A8}$$

where

$$A = \frac{3}{\mu_p[H^{(p)}]+2}. \tag{A9}$$

Solving the earlier equations for the magnetic moments requires specifying the structure of the suspension. Shkel and Klingenberg (2001) determined the magnetic moments self-consistently for the case of a suspension structure composed of well-separated chains of particles. Here we wish to determine the magnetic properties for a random suspension of particles. By symmetry, the average dipole moment is aligned with the applied field. The average moment magnitude can be obtained self-consistently by assuming that each sphere contributes equivalently to the magnetization of the suspensions [Adriani and Gast (1988)]. Ensemble averaging Eqs. (A4) and (A6) yields the following equation for the mean moment magnitude:

$$m = \alpha_m[H^{(p)}]H_0\left\{1+n\alpha_m[H^{(p)}]\int(\mathbf{h}\cdot\mathbf{T}\cdot\mathbf{h})g(\mathbf{r})dV\right\}^{-1}, \tag{A10}$$

where n is the particle number density, $\mathbf{h}$ is the unit vector in the direction of the applied field, and $g(\mathbf{r})$ is the pair distribution function. The earlier integral is conditionally convergent, but can be resolved using the renormalization procedure described by Jeffery (1973) and Adriani and Gast (1988). Employing this approach, and assuming the simple form for the pair distribution function

$$g(\mathbf{r}) = \begin{cases} 0 & |\mathbf{r}| \leqslant \sigma \\ 1 & |\mathbf{r}| > \sigma \end{cases}, \tag{A11}$$

yields the following expression for the average local field strength:

$$H_{\text{loc}} = \frac{H_0}{1-\beta[H^{(p)}]\phi}, \tag{A12}$$

and the self-consistent mean-field dipole moment magnitude

$$m = \frac{\alpha_m[H^{(p)}]H_0}{1-\beta[H^{(p)}]\phi}, \tag{A13}$$

where $\beta = \{\mu_p[H^{(p)}]-1\}/\{\mu_p[H^{(p)}]+2\}$, and $\phi = \pi\sigma^3 n/6$ is the particle volume fraction.

The suspension magnetization $\mathbf{M} = M\mathbf{h}$ is given by

$$M = nm. \tag{A14}$$

The applied magnetic flux density $\mathbf{B}_0$ is related to the applied magnetic field $\mathbf{H}_0$ by the suspension permeability μ_{susp}:

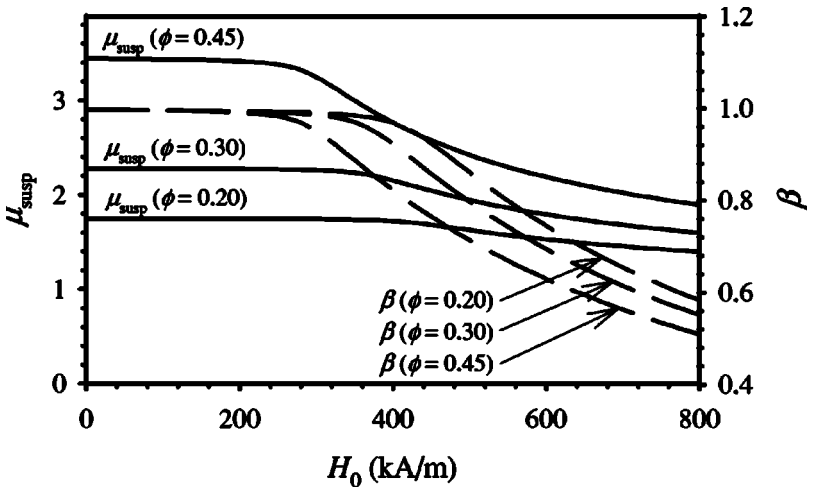

FIG. 12. Predicted magnetic properties μ_{susp} and β as a function of the applied magnetic field strength for $\phi = 0.20$, 0.30, and 0.45.

$$\mathbf{B}_0 = \mu_0(\mathbf{H}_0 + \mathbf{M}), \tag{A15}$$

$$= \mu_0 \mu_{\text{susp}} \mathbf{H}_0 . \tag{A16}$$

Combining Eqs. (A13)–(A16) yields the following expression for the suspension permeability:

$$\mu_{\text{susp}} = \frac{1 + 2\beta[H^{(p)}]\phi}{1 - \beta[H^{(p)}]\phi}. \tag{A17}$$

To determine μ_{susp} as a function of H_0 and ϕ, one must solve the nonlinear system of Eqs. (A1), (A8), (A9), and (A12), for the four unknowns, μ_p, $H^{(p)}$, A, and H_{loc}. Once these are determined, μ_{susp} can be calculated. In Fig. 12, μ_{susp} and β are plotted as a function of the applied magnetic field strength, H_0, for $\phi = 0.20$, 0.30, and 0.45. These results, along with those presented in Fig. 4, provide all the magnetic properties necessary to determine the Mason number of the homogeneous suspensions as a function of current.

References

Adriani, P. M., and A. P. Gast, ''A microscopic model for electrorheology,'' Phys. Fluids **31**, 2757–2768 (1988).

Aizawa, R., S. L. Vieira, M. Nakano, and Y. Asako, ''Hysteresis phenomenon in flow-curves of ER fluids containing sulfonated polymer particles,'' in *Proceedings of the 7th International Conference on Electro-rheological Fluids and Magneto-rheological Suspensions*, edited by R. Tao (World Scientific, Singapore, 2000), pp. 595–602.

Bossis, G., E. Lemaire, J. Persello, and L. Petit, ''Structuration and elasticity of electrorheological fluids,'' Prog. Colloid Polym. Sci. **89**, 1–5 (1992).

Bossis, G., Y. Grasselli, E. Lemaire, J. Persello, and L. Petit, ''Phase separation and flow-induced anisotropy in electrorheological fluids,'' Europhys. Lett. **25**, 335–340 (1994).

Bozorth, R. M., *Ferromagnetism* (van Nostrand, New York, 1951).

Bullough, W. A., J. Makin, A. R. Johnson, A. Hosseini-Sianaki, and R. Firooszian, ''ER shear characteristics: Volume fraction, shear rate, time response,'' J. Dyn. Syst., Meas., Control **118**, 221–225 (1996).

Carlson, J. D., and J. L. Sproston, ''Controllable fluids in 2000—Status of ER and MR fluid technology,'' *Actuator 2000—7th International Conference on New Actuators*, edited by H. Borgmann (Messe Bremen GmbH, Bremen, 2000), pp. 126–130.

Corbett, B., ''Riding the (magnetic) wave,'' Ward's Auto World **36**, 49 (2000).

Felt, D. W., M. Hagenbuchle, J. Liu, and J. Richard, ''Rheology of a magnetorheological fluid,'' J. Intell. Mater. Syst. Struct. **7**, 589–593 (1996).

Filisko, F. E., and S. Henley, ''Parameters affecting lamellar formations in ER fluids: An alternative model for ER activity,'' in *Proceedings of the 7th International Conference on Electro-Rheological Fluids and Magneto-Rheological Suspensions*, edited by R. Tao (World Scientific, Singapore, 2000), pp. 143–151.

Ginder, J. M., and L. C. Davis, ''Shear stresses in magnetorheological fluids: Role of magnetic saturation,'' Appl. Phys. Lett. **65**, 3410–3412 (1994).

Ginder, J. M., and S. L. Ceccio, ''The effect of electrical transients on the shear stresses in electrorheological fluids,'' J. Rheol. **39**, 211–234 (1995).

Henley, S., and F. E. Filisko, ''Flow profiles of electrorheological suspensions: An alternative model for ER activity,'' J. Rheol. **43**, 1323–1336 (1999).

Jeffery, D. J., ''Conduction through a random suspension of spheres,'' Proc. R. Soc. London, Ser. A **335**, 355–367 (1973).

Johnson, A. R., W. A. Bullough, R. Firoozian, A. Hosseini-Sianaki, J. Makin, and S. Xiao, ''Testing on a high speed electro-rheological clutch,'' in *Proceedings of the International Conference. Electrorheological Fluids: Mechanics, Structure, Technology and Applications*, edited by R. Tao (World Scientific, Singapore, 1992), pp. 424–441.

Klingenberg, D. J., ''Magnetorheology: Applications and challenges,'' AIChE J. **47**, 246–249 (2001).

Kordonski, W. I., and D. Golini, ''Fundamentals of magnetorheological fluid utilization in high precision finishing,'' in *Proceedings of the 7th International Conference on Electrorheological Fluids and Magneto-rheological Suspensions*, edited by R. Tao (World Scientific, Singapore, 2000), pp. 682–692.

Lewis, J., ''Put the brakes on pneumatics,'' Design News, July 5 (1999).

Martin, J. E., ''Thermal chain model of electrorheology and magnetorheology,'' Phys. Rev. E **63**, 011406 (2000).

Melrose, J. R., and D. M. Heyes, ''Simulations of electrorheological and particle mixture suspensions: Agglomerate and layer structures,'' J. Chem. Phys. **98**, 5873–5886 (1993).

Nakano, M., R. Aizawa, and Y. Asako, ''Steady and transient responses of electrorheological suspension passing through a rectangular channel,'' in *Proceedings of the Fifth International Conference on Electro-rheological Fluids, Magneto-rheological Suspensions and Associated Technology*, edited by W. A. Bullough (World Scientific, Singapore, 1996), pp. 132–139.

Nava, R., M. A. Ponce, L. Rejon, S. Viquez, and V. M. Castano, ''Response time and viscosity of electrorheological fluids,'' Smart Mater. Struct. **6**, 67–75 (1997).

Shkel, Y. M., and D. J. Klingenberg, ''Magnetorheology and magnetostriction of isolated chains of nonlinear magnetizable spheres,'' J. Rheol. **45**, 351–368 (2001).

Tanaka, K., T. Yoshida, and K. Koyama, ''Transient response of ER fluids,'' in *Proceedings of the International Conference. Electrorheological Fluids: Mechanics, Structure, Technology and Applications*, edited by R. Tao (World Scientific, Singapore, 1992), pp. 289–299.

Tanaka, K., A. Sahashi, R. Akiyama, and K. Koyama, ''Scaling behavior of response times of electrorheological suspensions with cation exchange resin particles,'' Phys. Rev. E **52**, R3325–R3328 (1995).

Vieira, S. L., M. Nakano, H. Henley, F. E. Filisko, L. B. Pompeo Neto, and A. C. F. Arruda, ''Transient behavior of the microstructure of electrorheological fluids in shear flow mode,'' in *Proceedings of the 7th International Conference on Electro-Rheological Fluids and Magneto-Rheological Suspensions*, edited by R. Tao (World Scientific, Singapore, 2000a), pp. 152–160.

Vieira, S., L. B. Pompeo Neto, and A. C. F. Arruda, ''Transient behavior of an electrorheological fluid in shear flow mode,'' J. Rheol. **44**, 1139–1149 (2000b).

Volkova, O., S. Cutillas, and G. Bossis, ''Shear banded flows and nematic-to-isotropic transition in ER and MR fluids,'' Phys. Rev. Lett. **82**, 233–236 (1999).

Volkova, O., G. Bossis, M. Guyot, V. Bashtovoi, and A. Reks, ''Magnetorheology of magnetic holes compared to magnetic particles,'' J. Rheol. **44**, 91–104 (2000).

von Pfeil, K., M. D. Graham, D. J. Klingenberg, and J. F. Morris, ''Pattern formation in flowing electrorheological fluids,'' Phys. Rev. Lett. **88**, 188301 (2002).

von Pfeil, K., ''A two-fluid continuum model for structure evolution in electro- and magnetorheological fluids,'' M.S. thesis, University of Wisconsin, Madison, WI, 2002.

von Pfeil, K., M. D. Graham, D. J. Klingenberg, and J. F. Morris, ''Structure evolution in electrorheological and magnetorheological suspensions from a continuum perspective,'' J. Appl. Phys. **93**, 5769–5779 (2003).